*Communication in Physical Sciences, 2023, 9(3): 367-382*

# Adsorption Efficiency of Scotch Bonnet Shells as a Precursor for Calcium Oxide Nanoparticles and an Adsorbent for the Removal of Amoxicillin from Aqueous Solution

**Anduang Ofuo Odiongenyi***, **Ubong Ime Essien, Emmanuel Jimmy Ukpong and Ifiok Okon Ekwere**

**Received: 06 May 2023/Accepted 20 July 2023/Published 24 July 2023**

*Abstract: Scotch Bonnet shells (BN) have high $CaCO_3$ content which was utilized in the synthesis of calcium oxide nanoparticles (CaONPS) for application in the adsorption removal of amoxicillin from water. The synthesized CaONPS showed adsorption in the UV region and displayed a band gap of 4.02 eV. It displayed high thermal stability and good crystalline properties with average crystalline size and macrostrain values of 5.67 nm and 0.3252. The crystalline size decreases as the macrostrain increases. The BET surface area of the CaONPS was evaluated as 785.04 $m^2/g$ while other pore properties such as pore diameter and pore volume were 2.65 nm and 0.1679 cc/g respectively. The nanomaterials showed strong evidence of a microporous nature, based on their particle size and the appearance of the SEM micrograph. The synthesized CaONPS showed strong adsorption efficiency for amoxicillin in water with efficiency approaching about 100 % under varying and influencing conditions such as pH, ionic strength, temperature, time and initial dye concentration. The adsorption system created by the CaONPS and the amoxicillin could be explained by the Langmuir adsorption isotherm, Pseudo second order kinetic model, intraparticle diffusion and thin film diffusion model.*

**Keywords**: Water contamination, antibiotics, remediation, adsorption, nanoparticles

**Anduang Ofuo Odiongenyi***
Department of Chemistry, Faculty of Physical Sciences, Akwa Ibom State University, Mkpat Enin, P. M. B. 1167, Uyo, Nigeria
**Email: anduangodiongenyi@aksu.edu.ng**

**Ubong Ime Essien**
Department of Chemistry, Faculty of Physical Sciences, Akwa Ibom State University, Mkpat Enin, P. M. B. 1167, Uyo, Nigeria

**Emmanuel Jimmy Ukpong**
Department of Chemistry, Faculty of Physical Sciences, Akwa Ibom State University, Mkpat Enin, P. M. B. 1167, Uyo, Nigeria.

**Ifiok Okon Ekwere**
Department of Chemistry, Faculty of Physical Sciences, Akwa Ibom State University, Mkpat Enin, P. M. B. 1167, Uyo, Nigeria

## 1.0 Introduction

The contamination of the global water systems has received tremendous research input because of the essential role water plays in several aspects of life such as agriculture, maintenance of life, industrial applications, etc (Odiongenyi *et al*., 2015). Cases of contamination arising from heavy metals, organic contaminants, dyes, crude oil and antibiotics have been widely reported (Odiongenyi, 2020, 2022; Ogoko, 2017; Osu and Ogoko, 2022). Given the extensive documented information on the dominance of contaminated water, measures towards remediation and abatement of the impact of contamination are of research significance.

Apart from water contamination, the management of non-biodegradable solid wastes (such as crustacean shells) has also created significant environmental impacts (Odoemelam and Eddy, 2009). Consequently, novel approaches arising from deep environmental innovation may be most significant if the management of solid wastes through resource recovery or recycling can create a solution for the management of contaminated water because raw materials cost would be extremely reduced in addition to the enhancement of multiple dimensional and dynamic solutions. In light of the stated information, current research has yielded some hopes in the conversion of crustacean shells to calcium-based nanoparticles for the remediation of contaminated water CaONPs (Habte *et al*., 2019; Kumari *et al*., 2023; Mostafa *et;*., 2023). The success is due to the content of $CaCO_3$ that dominates most crustacean shells (Gbenebor *et al*., 2016). Bonnet shell (See plate 1 below) is one of the known shells that is rich in $CaCO_3$. After the consumption of the flesh, the shells are usually disposed of as waste and since they are not biodegradable, they often constitute serious nuisance to the environment. It is in light of these challenges that this research seeks to synthesize CaONPS from bonnet shells for the remediation of amoxicillin-contaminated water. Amoxicillin is an antibiotic which has been classified among the emerging contaminants when present in water. Therefore, their removal is necessary to enhance the beneficial roles of water in the environment. Emerging contaminants such as amoxicillin are among the lists of contaminants that are billed to be given adequate need for their removal from the environment because of the future risk, they could pose.

**Plate 1: Photograph of Bonnet shells (BN)**

## 2.0 Materials and Methods

Samples of bonnet shells (BN) were obtained from a dumpsite around Ibeno in Akwa Ibom State. The samples were thoroughly washed dried and crushed to powdered form. The sol-gel method was adopted for the synthesis of the samples as reported elsewhere (Eddy *et al*., 2023a, b). 200 g of the powder sample was reacted with 2 M HCl to remove the carbon through conversion of the $CaCO_3$ to $CaCl_2$ and $CO_2$ (equation 1)

$$CaCO_3 + 2HCl \rightarrow CaCl_2 + H_2O + CO_2 \quad (1)$$

After the completion of the above reaction, the sample was washed severally with water to remove unreacted HCl and was dried for 24 hours. The dried sample was reacted with 50% NaOH solution to obtain $Ca(OH)_2$ gel (equation 2)

$$CaCl_2 + 2NaOH \rightarrow Ca(OH)_2 + 2NaCl \quad (2)$$

The $Ca(OH)_2$ was washed, dried and calcined in a muffle furnace at 700 °C for four hours to produce CaONPS (equation 3)

$$Ca(OH)_2 \rightarrow CaONPS \quad (3)$$

The water from the $Ca(OH)_2$ is consumed by the high-temperature furnace, leaving CaONPS as the only product.

### *2.1 Characterization of CaONPS*

UV- Shimadzu UV-Visible Spectrophotometer, model UV-1800 series

(UV analysis), Model PANalyticalX'PertPro (XRD profile), GA- PerkinElmer TGA-4000 (TGA and DTA) and BET- Nova4200e (nitrogen adsorption studies) were used for the characterization of the samples.

### 2.2 *Adsorption experiment*

A batch adsorption experiment was conducted as reported in the literature (Ogoko *et al*., 2023). Concentrations of the drug used for the investigation of the influence of the initial concentration of the drug were 10, 20, 30, 40 and 50 ppm. The effect of temperature was investigated within the range of 303 to 343 K while ionic strength was investigated using various concentrations of KCl within the range, of 0.01 to 0.1M and time between 10 and 70 minutes. In varying the listed factors, the concentration of the drug was fixed at 50 ppm. The spectrophotometric method was used to evaluate the percentage amount of drug absorbed after each experiment using equation 4

$$\%\, Removal = \frac{C_0 - C_e}{C_0} \times \frac{100}{1} \qquad (4)$$

where $C_0$ and Ce are the inlet and outlet concentrations of the drugs, repectively.

## 3.0 Results and Discussion

### *3.1 Characterization of the CaONPS*

Fig. 1a shows the UV visible spectrum of the nanoparticles with a displayed wavelength for maximum absorption at 306 nm which implies that the materials absorb in the visible light region (Odoemelam *et al*., 2023). Based on the Plank's equation, the bandgap of the material can be evaluated as follows (Eddy *et al*., 2022a)

$$E_{NG} = \frac{hc}{\lambda_{max}} \qquad (4)$$

The evaluated bandgap is 4.05 eV, which is comparable to values reported elsewhere (Eddy *et al*, 2023a-b).

The XRD spectrum presented in Fig. 1b. provided three sets of information on the character of the synthesized nanoparticles, including peak angle (and associated properties), crystalline size and microstrain. The most intense XRD peak for the nanoparticles was obtained at 29.50° while other peaks were XRD diffraction angles were obtained at 18.09, 28.77, 34.20 and 39.52 °.

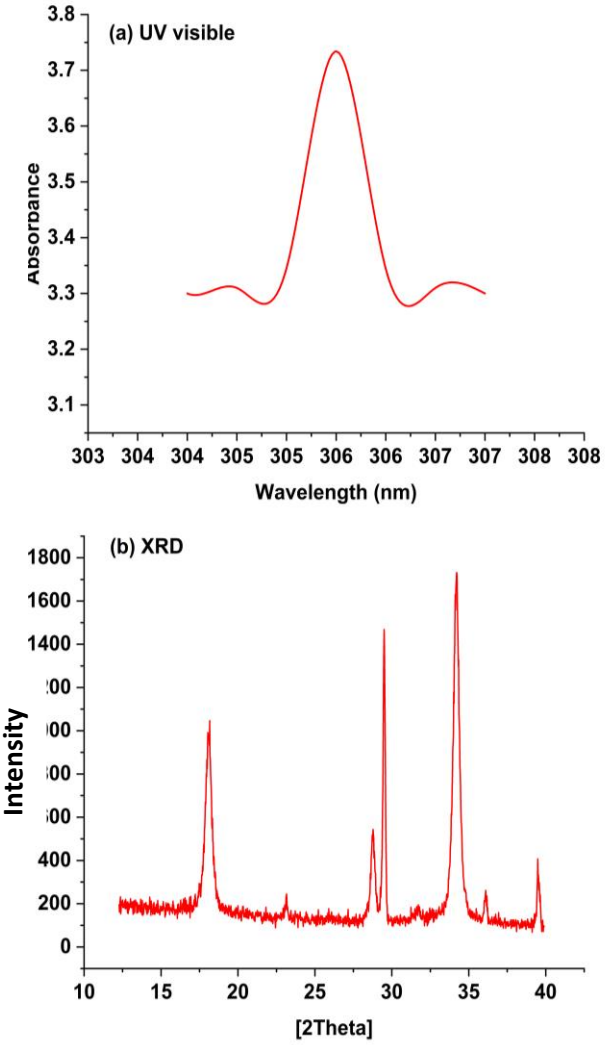


**Fig. 1: (a) UV visible spectrum (b) XRD spectrum of the synthesized CaONPS**

The major peak observed from the spectrum aligns with reported works on the crystallinity of CaONPS concerning the most intense peak (Safaei-Ghomi *et al*., 2013)

The Scherrer equation was used to characterize the samples regarding their crystalline size ($d_{cryst}$). The expression for the equation is given as follows (Eddy *et al*., 2023a)

$$d_{cryst} = \frac{k\lambda}{FWHM * cos\theta} \qquad (5)$$

where $\lambda$ is the wavelength of the CU-K line, which is numerically equal to 1.54 and k is the

Scherrer constant approximated as equal to 0.9. The equation gave a mean crystalline size of 5.67 nm which is lower than some values reported elsewhere for CaONPS including 112 nm (Khine *et al*., 2022), 24.34 (Jalu *et al*., 2021) and 35.93 nm (Mazher *et al*., 2023). The microstrain of the CaONPS was evaluated using equation 6 (Eddy *et al*., 2023b)

$$\varepsilon = \frac{\beta}{4\tan\theta} \quad (6)$$

The evaluated macrostrain is also recorded in Table 1 and it shows that it decreases with an increase in crystalline size, which defines a trend expected for some crystalline perfection (Depero *et al*., 1999).

**Table 1: XRD parameters for the CaONPS**

| 2θ | Width | Intensity | FWHM | $d_{cryst}$ $(nm)$ | ε |
|---|---|---|---|---|---|
| **18.09** | 0.3913 | 734.64 | 0.4607 | 3.04 | 0.7235 |
| **28.77** | 0.2379 | 345.60 | 0.2789 | 5.13 | 0.2719 |
| **29.50** | 0.1306 | 1175.98 | 0.1538 | 9.31 | 0.1460 |
| **34.19** | 0.3619 | 1402.46 | 0.4276 | 3.39 | 0.3476 |
| **39.52** | 0.1672 | 237.95 | 0.1969 | 7.47 | 0.1370 |

The Brunauer-Emmett-Teller (BET) principles in the determination of the dimension of nanoparticles are based on the principle of the capacity of the nanocomposite to adsorb nitrogen at various pressures, according to the BET model, given by equation 7 (Sinha *et al*., 2019),

$$\frac{1}{N[(P_0/P)-1]} = \frac{1}{N_m} + \frac{C-1}{N_m C}\left(\frac{P}{P_0}\right) \quad (7)$$

where N is the amount of nitrogen gas adsorbed at a pressure, P, while $N_m$ is the monolayer adsorption capacity, $P_0$ is the initial pressure, C is a constant that is related to the heat capacity. $C = [q_{ads} - q_{cond}]/RT$. $q_{ads}$ is the adsorption heat while $q_{cond}$ is the heat of condensation of the adsorbate. The multi-point BET plots (Fig. 2(a)) for the adsorption of nitrogen by the synthesized nanocomposite gave $R^2$ values of 0.9996 for calcium oxide nanoparticles synthesized from SB shells.

The multipoint BET surface areas (Multi-BET) of the nanocomposite particle were evaluated from the BET parameters using the following equation (Pomposo *et al*., 2009),

$$Mult - BET = \frac{1}{\frac{1}{X_m} + \frac{C-1}{X_m C}} * A \quad (8)$$

where A is the cross-sectional area of the adsorbate, which is approximately equal to 0.162, $m^2$ for nitrogen adsorption on CaONPs from the bonnet shell.

The particle size of the nanoparticles and other pore parameters was analysed using nitrogen adsorption isotherms according to Brauner-Emmett-Teller (BET) and Density functional theory (DFT) models and the results obtained are shown in Table 2. The BET plot is also shown as an example plot in Fig. 2.

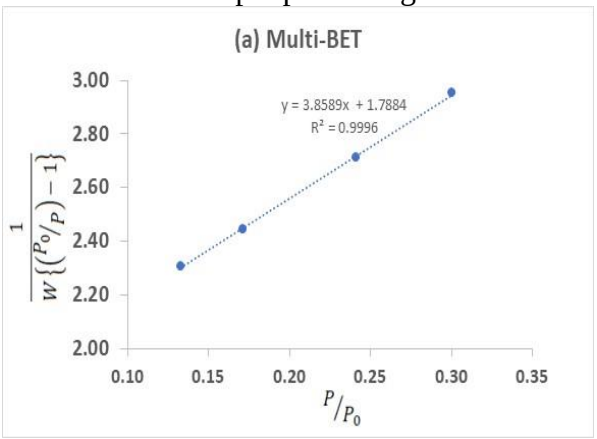


**Fig. 2: Multi-BET plot for the adsorption of nitrogen by the CaONPS**

The evaluated BET surface area is higher than values reported from some studies such as 748 $m^2/g$ reported by Mostafa, *et al*. (2023) 77.42 $m^2/g$ (Jalu *et al*. (2021) and 135 $m^2/g$ (Abdelatif *et al*., 2020). The particle size and pore volume

of the nanoparticles were evaluated from DFT analysis as 2.65 nm, which aligns with the microporous classification for the compound (Ogoko *et al*., 2023).

**Table 2: Pore properties of the synthesized CaONPS**

| Properties | Pore size (nm) | Pore Volume (cc/g) | Surface area ($m^2/g$) | PV/SA |
|---|---|---|---|---|
| **BET** | - | - | 785,04 | |
| **DFT** | 2.65 | 0.1679 | 139.00 | 4 575.64 |

The thermal stability of the nanoparticles was observed through TGA and DTA curves which are represented by Figs.3(a) and (b). The TGA curve shows initial changes corresponding to loss of water, followed by loss of adsorbed water before descending towards stability from around 800 °C. The DTA plot reveals similar information and confirms that the conversion process is endothermic.

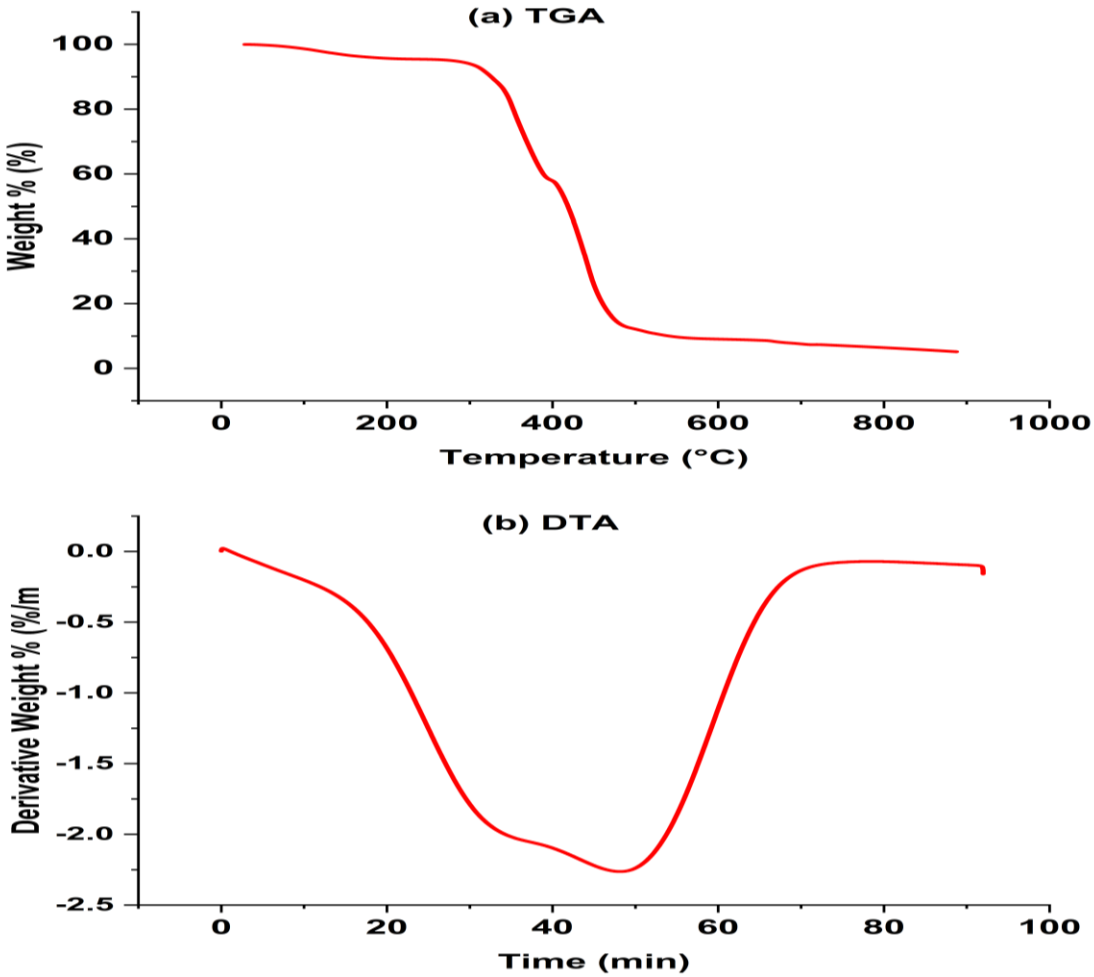


**Fig. 3: (a) TGA and DTA plots for the CaONPS**

The SEM micrograph of the BN shell synthesized CaONPS is shown in Fig. 4. The micrograph depicts spherical molecular shapes for the nanoparticles with some uneven packed-like structure, that may suggest some amorphous-like structure.

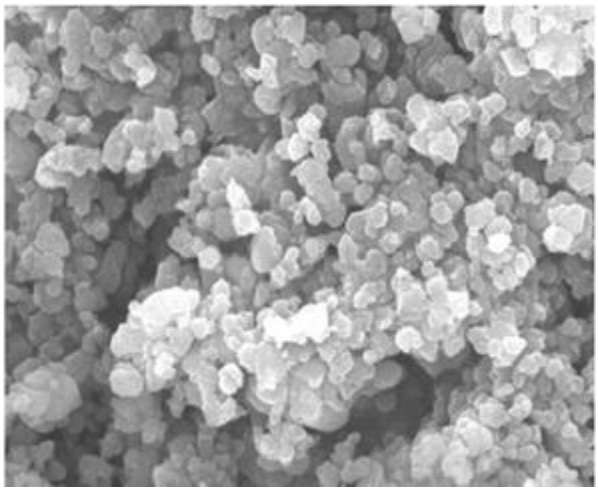

**Fig. 4: Scanning electron micrograph of the synthesized CaONPS**

### *3.2 Adsorption study*

The influence of the initial concentration of amoxicillin, time, ionic strength, pH and temperature on the adsorption removal of amoxicillin are shown in Fig.s 5 to 9 respectively. Fig. 5 reveals that the concentration of amoxicillin withdrawn from the solution by adsorption decreases with an increase in the initial concentration, which indicates that the available adsorption site provided by the CaONPS must have been progressively occupied as more drug molecules diffuse to the surface of the nanoparticles. The raw BN sample also showed a similar trend concerning the percentage of the drug removed and the initial concentration. However, the maximum removal by the raw sample was below 80% while the CaONPS showed an almost complete removal. An increase in adsorption as time increases (Fig. 6) reveals that the adsorbent becomes more effective as time ensures successful filling of the available adsorption sites. The raw samples of BN showed a reverse behaviour. Ionic strength (Fig. 7) was observed to exert increasing efficiency to the CaONPS as an adsorbent for the removal of amoxicillin showing an increasing trend up to 86% at KCl concentration of 0.1 M (Fig. 7). Such impact suggests the synergistic enhancement of adsorption due to the presence of halide ion (Odiongeneyi, 2019; Odiongenyi and Afangide, 2019). Fig. 8 shows that the optimum pH for the adsorption removal of amoxicillin by CaONPS is the acidic pH because adsorption showed a significant decline as the pH increased. The decrease was significantly more for the raw BN compared to the nano BN, which is evidence that the nanoparticles exhibit better surface properties than the crude sample. An increase in adsorption was observed as the temperature increased (Fig. 9) indicating that at higher temperatures, the surface of the adsorbent must have been activated, leading to the provision of more adsorption sites. Therefore, the optimum temperature was observed at 333 K while the trend supported the mechanism of chemical adsorption (Eddy and Ita, 2011).

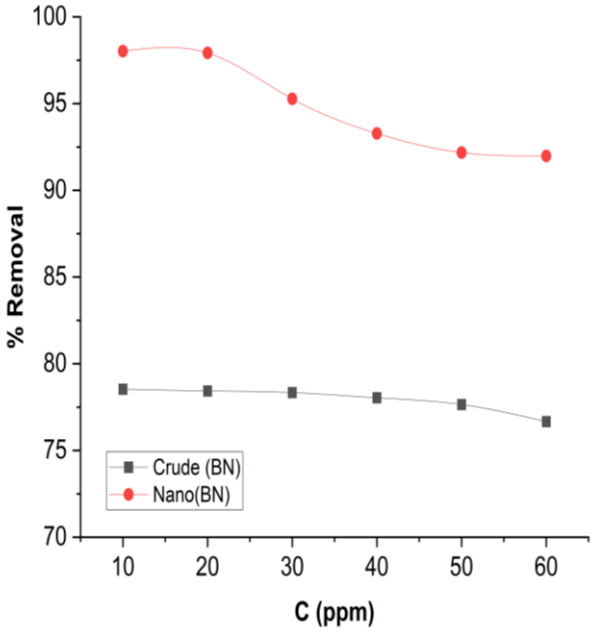


**Fig. 5: Variation of percentage amoxicillin removed by adsorption with Initial concentration of amoxicillin**

#### *3.2.1 Adsorption isotherm*

The testing of the fitness of different adsorption isotherms for the adsorption behaviour of the CaONPS confirmed the Langmuir isotherm as the best-fitted model,

which can be represented according to equation 9 (Condurache *et* al., 2022; Umeh *et al*., 2021)

$$\frac{C_e}{Q_e} = \frac{1}{k_L Q_{max}} + \frac{C_e}{Q_{max}} \quad (9)$$

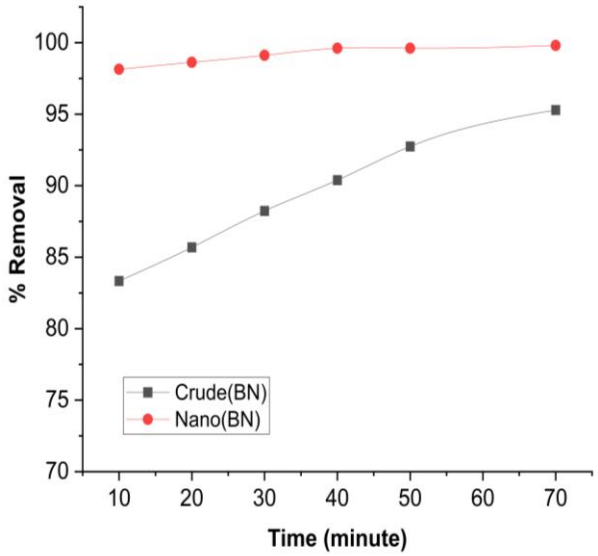


**Fig. 6: Variation of percentage amoxicillin removed by adsorption with time**

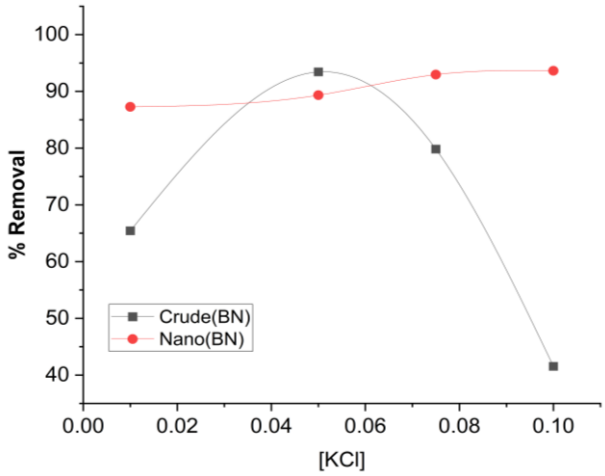


**Fig. 7: Variation of percentage amoxicillin removed by adsorption with ionic strength**

Based on the equation a plot of $\frac{C_e}{Q_e}$ against $C_e$ was linear for the investigated adsorbent (Fig. 10) and the extent of fitness was evaluated by the $R^2$ and error values as shown in Table 3. It is confirmed from the results that the best Langmuir maximum adsorption capacity ($Q_{max}$) was observed for the nanomaterials compared to the crude samples.

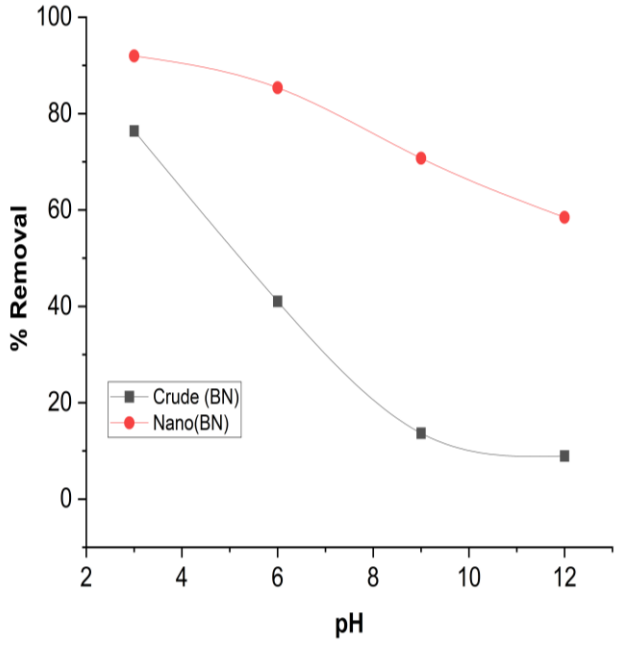


**Fg. 8: Variation of percentage amoxicillin removed by adsorption with pH**

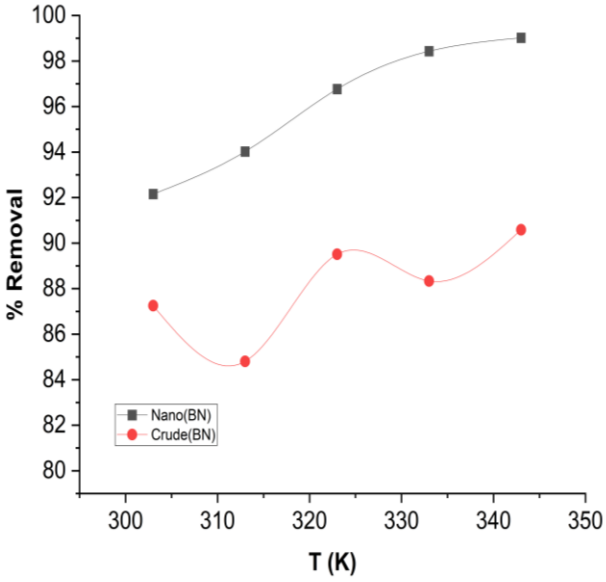


**Fg. 9: Variation of percentage amoxicillin removed by adsorption with temperature**

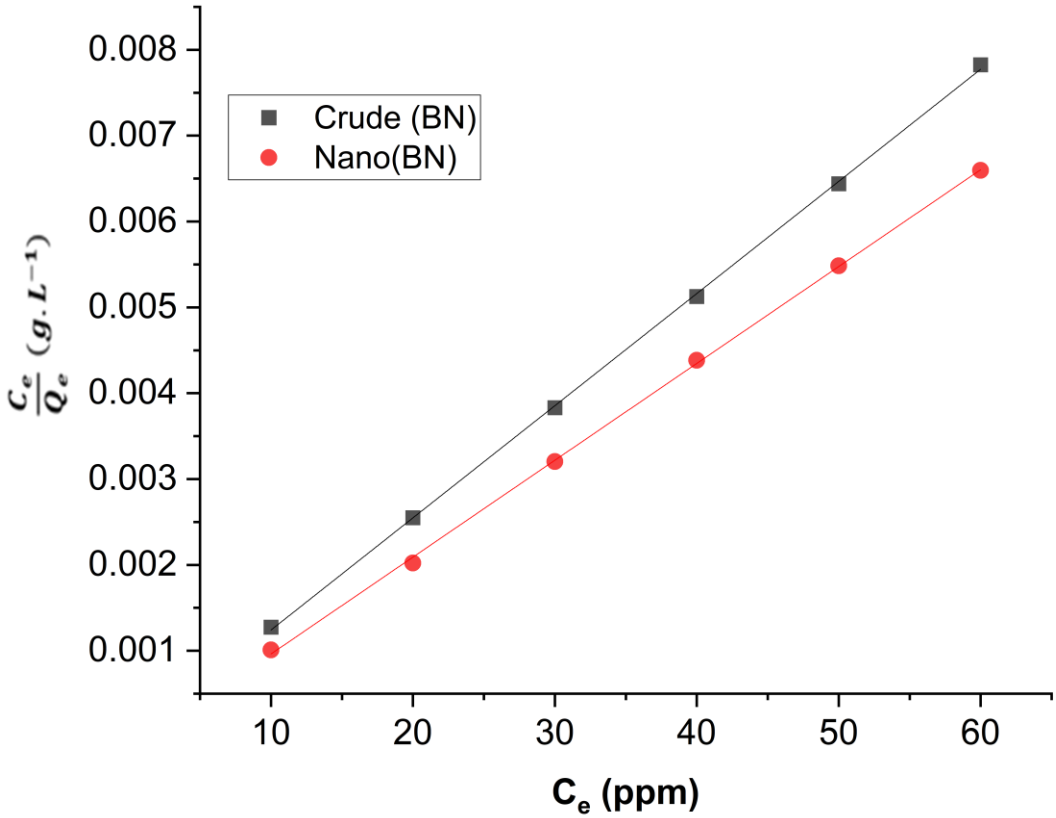


**Fig. 10: Langmuir isotherm for the adsorption of amoxicillin by the synthesized CaONPS**

The Nano(BN) gave $Q_{maz}$ of 7794.23 mg/g The observed maximum adsorption capacity is larger than the values reported for most CaO-based nanoparticles. For instance, Kumar *et al*. (2022) reported a Langmuir maximum adsorption capacity of 63 mg/g for the adsorption of naphthalene by CaONPs, Oruganti *et al*. (2022) also reported an adsorption maximum of 8.1 mg/g for ciprofloxacin adsorption by CaONPs while Oladoja *et al*. (2012) reported $Q_{max}$ of 225 mg/g for the adsorption of $Cr^{6+}$ by CaONPs. Generally, $Q_{max}$ varies with the method of synthesis, environmental conditions (such as temperature, pH, amount of adsorbate, the presence of other ions, initial amoxicillin concentration, etc.) and the type of adsorbate. The fitness of the slope values indicated lower error for all the adsorbents but better for the nanomaterials compared to the crude sample. The sum of square errors and mean square errors are low, indicating the reliability of the Langmuir adsorption model for the investigated adsorbents.

The thermodynamic parameters for the adsorption of amoxicillin by the adsorbent was deduced using the Transition state equation (Equation 10) (Odoemelam *et al*., 2018)

$$lnk_{eq} = \frac{\Delta S}{R} - \frac{\Delta H}{RT} \quad (10)$$

In equation 10, $k_{eq}$ is the equilibrium constant of adsorption and was evaluated as a quotient of the concentration of the drug adsorbed ($C_{ads}$) to the equilibrium concentration of the drug ($C_e$), which is according to equation 11

$$k_{eq} = \frac{C_{ads}}{C_e} \quad (11)$$

Consequently, equation 11 can be rewritten as equation 12.

$$ln\left(\frac{C_{ads}}{C_e}\right) = \frac{\Delta S}{R} - \frac{\Delta H}{RT} \quad (12)$$

Equation 12 is a linear model, hence a plot of $ln\left(\frac{C_{ads}}{C_e}\right)$ against 1/T describes a Transition state plot with entropy change (ΔS) equal to the product of the intercept and the gas constant (R) while enthalpy change (ΔH) would be equal to be the product of the slope and the gas constant. A plot of $ln\left(\frac{C_{ads}}{C_e}\right)$ with 1/T was linear (plot not shown) and thermodynamic and reliability parameters deduced from the plots are recorded in Table 4. The evaluated values (Table 4) indicated that the adsorption is exothermic (because of negative values of enthalpy change) concerning the nanoparticles but exothermic for the crude materials.

**Table: 3: Langmuir and Statistical parameters deduced from the Langmuir adsorption isotherm for crude and CaONPs from BN**

| Parameter | CaONPs | Crude |
|---|---|---|
| | Nano(BN) | Crude (BN) |
| **Slope ± SE** | $1.1283 \times 10^{-4} \pm 0.000001108$ | $1.3067 \times 10^{-4}$ 0.0000009552 |
| **Intercept** | $1.6607 \times 10^{-4} \pm 0.00004318$ | $5.535 \times 10^{-3} \pm 0.000003720$ |
| **$R^2$** | 0.9996 | 0.9998 |
| **$Q_{max}$ $(mg/g)$** | 7794.23 | 7526.87 |
| **$k_L$ $(min^{-1})$** | 0.6794 | 0.0231 |
| **SS** | 0.00002228 | 0.002228 |
| **MS** | 0.002228 | 0.002228 |
| **SSE** | 0.00000000803 | 0.00000000803 |
| **MSE** | 0.000000002151 | 0.000000002151 |

The change in enthalpy was also very low and suggests that the adsorption favours the physisorption mechanism. The results also reveal higher $R^2$ values and a lower sum of square error as well as mean square error for the data representing the nanomaterials than their corresponding precursor (crude). The irregular pattern of plots was also observed for the crude samples but those representing the corresponding nanomaterials are well-defined linear plots.

### 3.3 Kinetic of the adsorption

The fitness of the pseudo-order reaction was also tested for the adsorption of amoxicillin on the investigated adsorbents. The test results confirmed the suitability of the pseudo-second-order kinetic, based on equation 13 (Odoemelam *et al*., 2023)

$$Q_t = \frac{k_2 Q_e^2 t}{1 + k_2 Q_e t} \quad (13)$$

The reciprocal of the above equation gives equation 14

$$\frac{1}{Q_t} = \frac{1}{k_2 Q_e^2 t} + \frac{k_2 Q_e t}{k_2 Q_e^2 t} \quad (14)$$

The simplification of equation 14 leads to equation 15 and finally equation 16 when both sides of the equation are multiplied by time, t

$$\frac{1}{Q_t} = \frac{1}{k_2 Q_e^2 t} + \frac{1}{Q_t} \quad (15)$$

$$\frac{t}{Q_t} = \frac{1}{k_2 Q_e^2} + \frac{t}{Q_e} \quad (16)$$

Linear evaluation of equation 16. is consequential with a plot of $\frac{t}{Q_t}$ versus t in order to obtain a slope = $\frac{1}{Q_e}$and intercept equal to $\frac{1}{k_2 Q_e^2}$ as shown in Fig. 11. Variables deduced from the plots are recorded in Table 5. The results reveal a high degree of fitness for all the

adsorbents while the evaluated equilibrium amounts of the drug adsorbed by the nanoparticles are higher for the nanoparticles (Table 5) than the crude materials. The rate constants for the nanoparticles are also higher which suggests that the adsorption of the drug by the nanoparticles is faster than the adsorption by the crude samples.

**Table 4: Transition and Statistical parameters deduced from the Langmuir adsorption isotherm for crude and CaONPs from BN, SN and C**

| Parameter | CaONPs | Crude |
|---|---|---|
| | Nano(BN) | Crude (BN) |
| Slope ± SE | -1.2686±0.05437 | 1.0217±3.11114 |
| Intercept | 5.7478 ±0.16873 | 0.3071±9.65457 |
| $R^2$ | 0.9945 | 0.0347 |
| $\Delta H\ (J/mol)$ | -10.5471 | 8.4944 |
| $\Delta S\ (J/mol)$ | 47.7872 | 2.5532 |
| SS | 0.16094 | 0.10438 |
| MS | 0.16094 | 0.10438 |
| SSE | 0.000886868 | 2.90376 |
| MSE | 0.0002956 | 0.96792 |

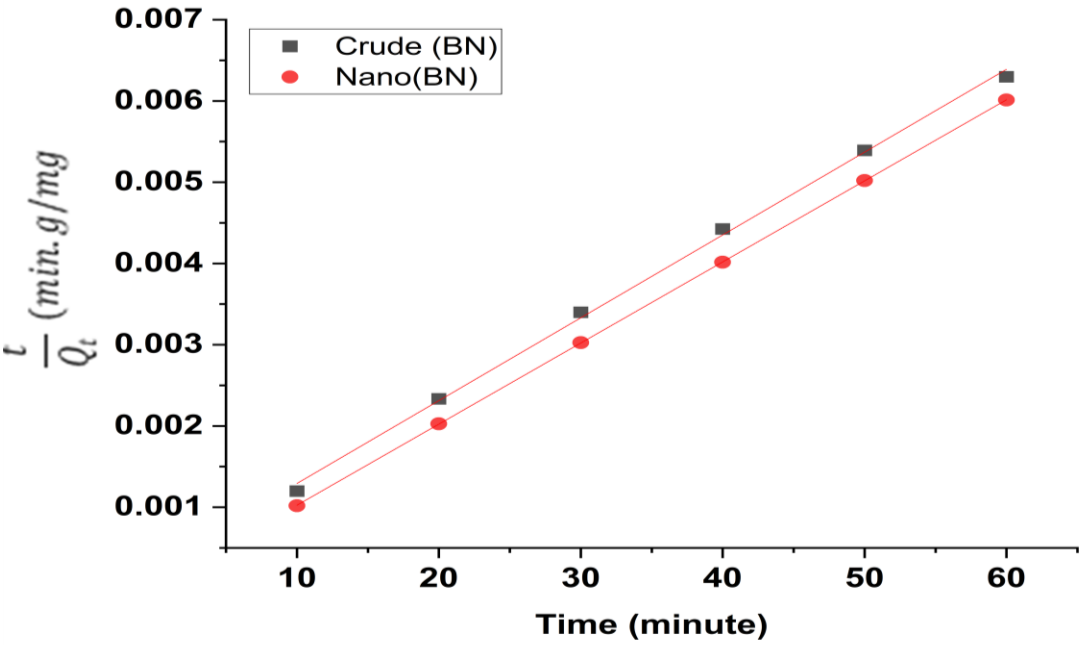


**Fig. 11: Pseudo second order plot for the adsorption of amoxicillin by CaONPS**

The fitness of the intraparticle diffusion model was also investigated, based on equation 16, which expects a linear plot for values of $Q_t$ against the square root of the corresponding time, t. Such plots, covey information on the dominancy of the intraparticle diffusion if the intercept, C is equal to zero, otherwise, film diffusion (equation 17) may interplay

$$Q_t = k_{int} t^{\frac{1}{2}} + C \quad (16)$$

$$-\ln\left(1-\left(\frac{Q_t}{Q_e}\right)\right) = k_{LF}t + C \quad (17)$$

The plot of $Q_t$ against $t^{\frac{1}{2}}$ (Fig. 13) was not a zero-intercept plot, hence the liquid film diffusion plot of $-\ln\left(1-\left(\frac{Q_t}{Q_e}\right)\right)$ versus t was also developed. Parameters deduced from the intraparticle diffusion model are presented in Table 6 while Table 7 presents similar data for the liquid film diffusion plot. Both sets of graphs showed an excellent degree of fitness but based on the evaluated rate constant, intraparticle diffusion of the adsorbate unto the adsorbent exerted a greater influence than the liquid film diffusion. Although the relative contribution of liquid film diffusion seems to be minimal, since the intercepts are not equal to zero, it is confirmed that liquid film diffusion has some contribution towards the mass transportation of the drug to the surface of the adsorbent. It is worth stating that the adsorption on the surface of the nanoparticles showed better model fitness than the crude adsorbent

**Table 5: Kinetics and statistical parameters for the adsorption of amoxicillin by crude and CaONPs from BN**

| Parameter | CaONPs | Crude |
|---|---|---|
| | **Nano(BN)** | **Crude (BN)** |
| **Slope ± SE** | $9.9796 \times 10^{-5} \pm 1.310 \times 10^{-7}$ | $1.019 \times 10^{-3} \pm 2.0157 \times 10^{-6}$ |
| **Intercept** | $2.7260 \times 10^{-5} \pm 5.1018 \times 10^{-6}$ | $2.7334 \times 10^{-4} \pm 7.8501 \times 10^{-5}$ |
| **$R^2$** | 0.9999 | 0.9984 |
| $Q_e\ (mg/g)$ | 10020.44 | 981.35 |
| $k_2(min^{-1})$ | $3.6759 \times 10^{8}$ | $3.589 \times 10^{6}$ |
| **SS** | $1.7429 \times 10^{-5}$ | $1.8184 \times 10^{-5}$ |
| **MS** | $1.7429 \times 10^{-5}$ | $1.81843 \times 10^{-5}$ |
| **SSE** | $1.2013 \times 10^{-10}$ | $2.8442 \times 10^{-8}$ |
| **MSE** | $3.0033 \times 10^{-11}$ | $7.1105 \times 10^{-9}$ |

.**Table 6: Intraparticle diffusion model kinetics and statistical parameters deduced from the Langmuir adsorption isotherm for crude and CaONPs from BN**

| Parameter | CaONPs | Crude |
|---|---|---|
| | **Nano(BN)** | **Crude (BN)** |
| **Slope ± SE** | 0.00109±0.0000669151 | 0.00112±0.0000481892 |
| **Intercept** | 0.0027±0.000395875 | -0.00254±0.000285091 |
| **$R^2$** | 0.9852 | 0.9926 |
| $k_{int}\ (/min)$ | 0.00109±0.0000669151 | 0.00112±0.0000481892 |
| $C$ | -0.0027±0.000395875 | -0.00254±0.000285091 |
| **SS** | 0.00001717 | 0.0000180785 |
| **MS** | 0.00001717 | 0.0000180785 |
| **SSE** | 0.000000258856 | 0.000000134249 |
| **MSE** | 0.0000000647139 | 0.0000000335621 |

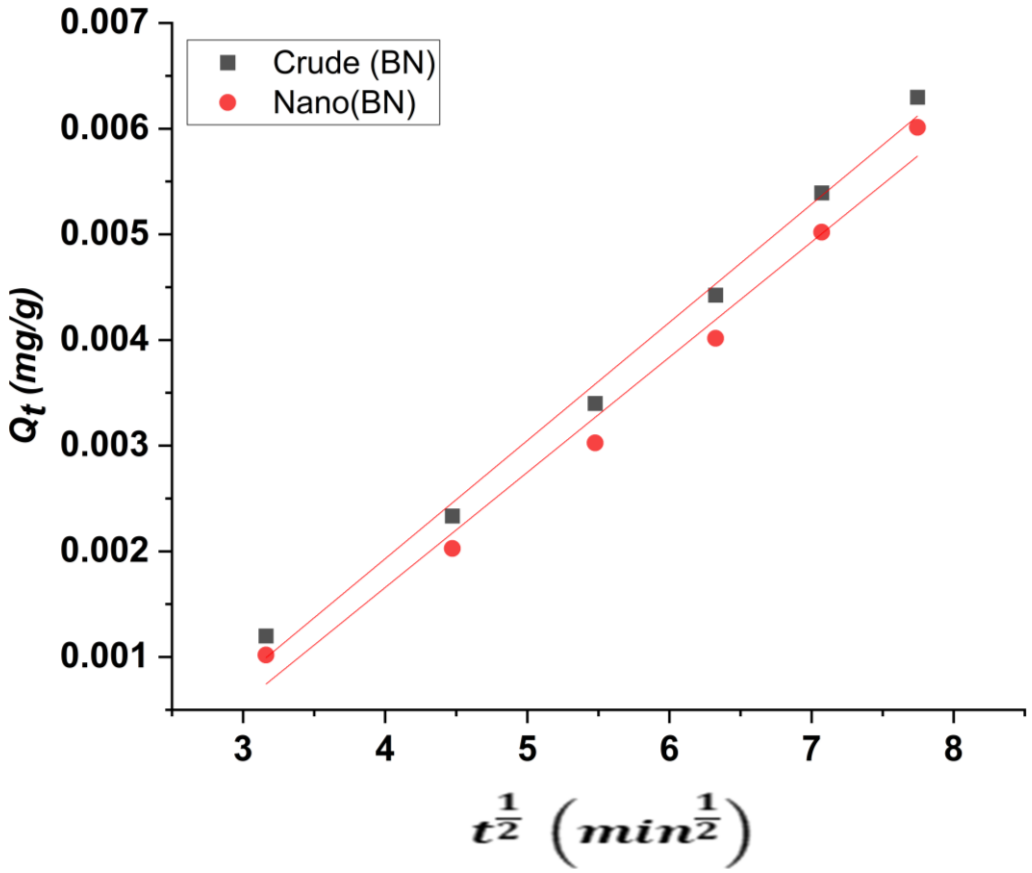


**Fig. 13: Intraparticle diffusion plot describing the kinetics of the adsorption of amoxicillin on CaONPS**

**Table: 7 Liquid film diffusion model kinetics and statistical parameters deduced from the Langmuir adsorption isotherm for crude and CaONPs from BN**

| Parameter | CaONPs | Crude |
|---|---|---|
| | Nano(BN) | Crude (BN) |
| Slope ± SE | 0.0000690651±0.0000101112 | 0.14067±0.02165 |
| Intercept | -0.44891±0.000393773 | 12.26041±0.8433 |
| $R^2$ | 0.9210 | 0.9134 |
| $k_{LF}$ $(/min)$ | 0.0000690651±0.0000101112 | 0.14067±0.02165 |
| $C$ | -0.44891±0.000393773 | 12.26041±0.8433 |
| SS | 0.00000834748 | 34.63008 |
| MS | 0.00000834748 | 34.63008 |
| SSE | 0.000000715648 | 3.28225 |
| MSE | 0.000000178912 | 0.82056 |

## 4.0 Conclusion

The study indicates that BN shell has enough concentration of $CaCO_3$ that enables it to be a precursor for the synthesis of CaONPS. The synthesized nanoparticles show excellent surface properties, that support their suitability

for adsorption removal of amoxicillin from contaminated water. The performance of the nanoparticles outranged that of the crude samples in all the tested studies. It is possible to completely remove amoxicillin from contaminated water using this adsorbent. However, the recommendation of further application as a photocatalyst for the insurance of complete degradation of the drug to harmless forms is supported by the low bandgap function possessed by the nanoparticles.

## 5.0 References


Abdelatif, Y., Gaber, A.. A. M., Fouda, A. E. A. S. & Alsoukarry, T. (2020). Evaluation of Calcium Oxide Nanoparticles from Industrial Waste on the Performance of Hardened Cement Pastes: Physicochemical Study. *Processes*, *8*, 401. https://doi.org/10.3390/pr8040401

Condurache, B. C., Cojocaru, C., Samoila, P., Cosmulescu, S.F., Predeanu, G., Enache, A. C. & Harabagiu, V. (2022). Oxidized biomass and Its Usage as Adsorbent for Removal of Heavy Metal Ions from Aqueous Solutions. Molecules 27, 6119. https://doi.org/10.3390/molecules27186119.

Depero, L. E., Sangaletti, L., Allieri, B., Bontempi, E.& Zocchi, M. M. (1999). Correlation between crystallite sizes and microstrains in TiO2 nanopowders. *Journal of Crystal Growth*, 198-199, 1, pp. 516-520, https://doi.org/10.1016/S0022-0248(98)01086-0.

Eddy, N. O. & Ita, B. I. (2011). Theoretical and experimental studies on the inhibition potentials of aromatic oxaldehydes for the corrosion of mild steel in 0.1 M HCl. *Journal of Molecular Modeling* 17, pp. 633-647. DOI:10.1007/s00894-010-0749

Eddy, N. O., Garg, R., Garg, R., Aikoye, A. Ita, B. I. (2022b). Waste to resource recovery: mesoporous adsorbent from orange peel for the removal of trypan blue dye from aqueous solution. *Biomass Conversion and Biorefinery*, DOI: 10.1007/s13399-022-02571-5.

Eddy, N. O., Garg, R., Garg, R., Eze, S. I., Ogoko, E. C., Kelle, H. I., Ukpe, R. A., Ogbodo, R. & Chijoke, F. (2023b). Sol-gel synthesis, computational chemistry, and applications of Cao nanoparticles for the remediation of methyl orange contaminated water. Advances in Nano Research, https://doi.org/10.12989/anr.2023.15.1.000

Eddy, N. O., Odiongenyi, A. O., Garg, R., Ukpe, R. A., Garg, R., El Nemir, A., Ngwu, C. M. & Okop, I. J. (2023a). Quantum and experimental investigation of the application of *Crassostrea gasar* (mangrove oyster) shell–based CaO nanoparticles as adsorbent and photocatalyst for the removal of procaine penicillin from aqueous solution. *Environmental Science and Pollution Research*, doi:10.1007/s11356-023-26868-8.

Eddy, N. O., Ukpe, R. A., Ameh, P., Ogbodo, R., Garg, R. & Garg, R. (2022a). Theoretical and experimental studies on photocatalytic removal of methylene blue (MetB) from aqueous solution using oyster shell synthesized CaO nanoparticles (CaONP-O). Environmental Science and Pollution Research, https://doi.org/10.1007/s11356-022-22747-w.

Gbenebor, O. P., Adeosun, S. O., Lawal, G. I. & Jun, S. (2016). Role of $CaCO_3$ in the physicochemical properties of crustacean-sourced structural polysaccharides. *Materials Chemistry and Physics*,184, pp.203-209,https://doi.org/10.1016/j.matchemphys.2016.09.043.

Habte, L., Shiferaw, N., Mulatu, D., Thenepalli, T., Chilakala, R. & Ahn, J.W. (2019). Synthesis of Nano-Calcium Oxide from Waste Eggshell by Sol-Gel

Method. *Sustainability, 11*, 3196. https://doi.org/10.3390/su11113196.

Jalu, R. G., Chamada,T. A. and Kasirajan, R. (2021). Calcium oxide nanoparticles synthesis from hen eggshells for removal of lead (Pb(II)) from aqueous solution. Environmental Challenges. 4, https://doi.org/10.1016/j.envc.2021.100193.

Khine, E. E., Koncz-Horvath, D., Kristaly, F. *et al.* (2022). Synt hesis and characterization of calcium oxide nanoparticles for $CO_2$ capture. *J Nanopart Res, 24, 139,* https://doi.org/10.1007/s11051-022-05518-z.

Kumar, J. A., Krithiga, T., Narendrakumar, G., Prakash, P., Balasankar, K., Sathish, S., Prabu, D., Pushkala, D. P., Marraiki, N., Ramu, A. G., & Choi, D. (2022). Effect of $Ca^{2+}$ ions on naphthalene adsorption/desorption onto calcium oxide nanoparticle: Adsorption isotherm, kinetics and regeneration studies. *Environmental Research*. 12070. doi: 10.1016/j.envres.2021.112070.

Kumari, M., Sarkar, B. & Mukherjee, K. (2023). Nanoscale calcium oxide and its biomedical applications: A comprehensive review. *Biocatalysis and Agricultural Biotechnology*, 47, https://doi.org/10.1016/-j.bcab.2022.102506.

Mazher, M., Ishtiaq, M., Hamid, B., Haq, S. M., Mazhar, A., Bashir, F., Mazhar, M., Mahmoud, E.A., Casini, R., Alataway, A., et al. (2023). Biosynthesis and Characterization of Calcium Oxide Nanoparticles from *Citrullus colocynthis* Fruit Extracts, Their Biocompatibility and Bioactivities. *Materials*, 16, 2768. https:// -doi.org/10.3390/ma16072768.

Mostafa, F. A., Gad, A. N., Gaber, A A.M. *et al. (2023).* Preparation, characterization and application of calcium oxide nanoparticles from waste carbonation mud in clarification of raw sugar melt. *Sugar Tech*, *25*, pp. 331–338 (2023). https://doi.org/10.1007/s12355-022-01150-2

Mostafa, F.A., Gad, A.N., Gaber, AA.M. & Abdel-Wahap, A. (2023). Preparation, Characterization and Application of Calcium Oxide Nanoparticles from Waste Carbonation Mud in Clarification of Raw Sugar Melt. *Sugar Tech*., 25, pp. 331–338, https://doi.org/10.1007/s12355-022-01150-2.

Nayar, P., Waghmare, S., Nageshwar, P., Najar, M., Singh, U. & Agnihotri, A. (2021). Preparation of calcium oxide nanoparticles from industry rejects: Recovery and value addition of mineral values. *Materials Today: Proceedings*, 39, 4, pp. 1722-1726, https://doi.org/ -10.1016/j.matpr.2020.06.300.

Odiongenyi, A. O. (2019). Removal of ethyl violet dye from aqueous solution by graphite dust and nano graphene oxide synthesized from graphite dust. Communication in Physical Sciences, 4, 2, 10, pp. 103-109.

Odiongenyi, A. O. (2020). Utilization of *Musa cecropiodesi* woood saw dust for the removal of dispersed yellow (DY) dye from aqueous solution. *Communication in Physical Sciences* 5, 3, pp. , 270-280.

Odiongenyi, A. O. (2022). Influence of sol gel conversion on the adsorption capacity of crab shell for the removal of crystal violet from aqueous solution. *Communication in Physical Science*, 8,1, pp. 121-127.

Odiongenyi, A. O. & Afangide, N. R. (2019). Adsorption and thermodynamic studies on the removal of congo red dye from aqueous solution by alumina and nano-alumina. Communication in Physical Sciences, 4, 1, pp. 1-7.

Odiongenyi, A. O., Okon, J. O. J. and Enengedi, I. (2015). Assessment of the quality of packaged water in Uyo metropolis: South eastern Nigeria. *Journal International Journal of Chemical,*

*Materials and Environmental Research*, 1, 1, pp. 12-15.

Odoemelam, S. A. & Eddy, N. O. (2009). Studies on the use of oyster, snail and periwinkle shells as adsorbents for the removal of $Pb^{2+}$ from aqueous solution. *E. Journal of Chemistry* 6, 1, pp. 213-222.

Odoemelam, S. A., Emeh, N. U. & Eddy, N. O. (2018). Experimental and computational Chemistry studies on the removal of methylene blue and malachite green dyes from aqueous solution by neem (*Azadiractha indica*) leaves. Journal of Taibah University of Science, 12, 3, pp. 255–265, doi.org/10.1080/16583655.2018.1465725.

Odoemelam, S. A., Oji, E. O., Eddy, N. O., Garg, R., Garg, R., Islam, S., Khan, M. A., Khan, N. A. & Zahmatkesh, S. (2023). Zinc oxide nanoparticles adsorb emerging pollutants (glyphosate pesticide) from aqueous solution. *Environmental Monitoring and Assessment*, https://doi.org/10.1007/s10661-023-11255-0.

Odoemelam, S. A., Oji, E. O., Eddy, N. O., Garg, R., Garg, R., Islam, S., Khan, M. A., Khan, N. A. & Zahmatkesh, S. (2023). Zinc oxide nanoparticles adsorb emerging pollutants (glyphosate pesticide) from aqueous solution. *Environmental Monitoring and Assessment*, https://doi.org/10.1007/s10661-023-11255-0.

Ogoko, E. (2017). Physicochemical properties and heavy metal concentration of groundwater in Owerri metropolis, Nigeria. Current Journa of Applied Sciences and Tehnology, 23, 1, pp. 1-18.

Ogoko, E. C., Kelle, H. I., Akintola, O. & Eddy, N. O. (2023). Experimental and theoretical investigation of *Crassost - rea* gigas (gigas) shells based CaO nanoparticles as a photocatalyst for the degradation of bromocresol green dye (BCGD) in an aqueous solution. *Biomass Conversion and Biorefinery*. https://doi.org/10.1007/s13399-023-03742-8

Oladoja, N. A., Ojolade, I. A., Olaseni, S. E., Olatujoye, V. O., Jegede, O. S. & Agunloye, A. O. (2012). Synthesis of nano calcium oxide from a gastropod shell and the performance evaluation for Cr (VI) removal from aqua system. *Industrial & Engineering Chemistry Research*, *51*, 2, pp. 639-648, doi: 10.1021/ie201189z

Oladoja, N. A., Ojolade, I. A., Olaseni, S. E., Olatujoye, V. O., Jegede, O. S. & Agunloye, A. O. (2012). Synthesis of nano calcium oxide from a gastropod shell and the performance evaluation for Cr (VI) removal from aqua system. *Industrial & Engineering Chemistry Research*, *51*, 2, pp. 639-648, DOI: 10.1021/ie201189z

Oruganti, R. K., Pal, D., Panda, T. K. *et al.* (2022). Green synthesis of calcium oxide nanoparticles impregnated activated carbon from algal–bacterial activated sludge: its application in ciprofloxacin removal. *Int. J. Environ. Sci. Technol.*, https://doi.org/10.1007/s13762-022-04662-2.

Osu, C. I & Ogoko, E. C. (2022). Concentration levels of physicochemical parameters, nitrate and nitrite anions of floodwaters from selected areas in Port-Harcourt metropolis, Nigeria. Journal of Applied Sciences in Environmental Sanitation. 7, 2, pp. 147-152.

Safaei-Ghomi, J., Ghasemzadeh, M. A. & Mehrabi, M. (2013). Calcium oxide nanoparticles catalyzed one-step multicomponent synthesis of highly substituted pyridines in aqueous ethanol media. Scientia Iranica, 20, 3, pp. 549-554,https://doi.org/10.1016/j.scient.2012.12.037.

Umeh, T.C., Nduka, J.K. and Akpomie, K. G. (2021). Kinetics and isotherm modeling of Pb(II) and Cd(II) sequestration from polluted water onto tropical ultisol obtained

from Enugu Nigeria. *Appl Water Sci* **11**, 65, https://doi.org/10.1007/s13201-021-01402-8

**Declarations**

The authors declare that they have no conflict of interest.

**Data availability**

All data used in this study will be readily available to the public.

**Consent for publication**

Not Applicable

**Availability of data and materials**

The publisher has the right to make the data Public.

**Competing interests**

The authors declared no conflict of interest.

**Funding**

There is no source of external funding

**Authors' contributions**

AOO conceived the work and supervised the draft manuscript. EJU co-supervised the work, IOE read through and UIE carried out the experimental aspect of the work under the supervision of AOO.